ELSEVIER

Biophysical Chemistry 120 (2006) 225–236

Biophysical Chemistry

http://www.elsevier.com/locate/biophyschem

Model for kinetics of myosin-V molecular motors

Ping Xie *, Shuo-Xing Dou, Peng-Ye Wang

Laboratory of Soft Matter Physics, Beijing National Laboratory for Condensed Matter Physics, Institute of Physics, Chinese Academy of Sciences, Beijing 100080, China

Received 7 September 2005; received in revised form 22 November 2005; accepted 22 November 2005
Available online 28 December 2005

Abstract

A hand-over-hand model is presented for the processive movement of myosin-V based on previous biochemical experimental results and structural observations of nucleotide-dependent conformational changes of single-headed myosins. The model shows that the ADP-release rate of the trailing head is much higher than that of the leading head, thus giving a 1 : 1 mechanochemical coupling for the processive movement of the motor. It explains well the previous finding that some 36-nm steps consist of two substeps, while other 36-nm steps consist of no substeps. Using the model, the calculated kinetic behaviors of myosin-V such as the main and intermediate dwell time distributions, the load dependence of the average main and intermediate dwell time and the load dependence of occurrence frequency of the intermediate state under various nucleotide conditions show good quantitative agreement with previous experimental results.

Keywords: Myosin-V; Mechanism; Molecular motor; Kinetics

1. Introduction

Myosin-V is demonstrated to be able to move processively along helical actin filament and is involved in different forms of the intracellular transport [1]. It is composed of two heavy chains, each consisting of a motor domain and a neck domain having 6 IQ motifs bound with 6 light chains, an α-helical coiled coil and a global cargo-binding tail domain. It moves towards the barbed end of actin for at least 40–50 steps of ~36 nm without dissociating [2]. By using various experimental methods, many aspects of its kinetic and dynamic behaviors have been elucidated [2–12]. In particular, its kinetic behaviors such as the average moving velocity, the dwell time distribution, the average dwell time under various loads and nucleotide states have been systematically studied by using optical trapping nanometry [2,4,11]. Recently, it has also been revealed that there are two pathways for the 36-nm steps, one with 12- and 24-nm substeps, and the other without substeps [11].

Although it has been definitely determined that myosin-V moves along actin in a hand-over-hand manner [9], the microscopic mechanism of its processive movement has not been completely clear. Based on the lever arm mechanism that was originally proposed for muscle myosin II [13], many models have been proposed [4–6,8–12,14–16]. For quantitative study of the kinetics of molecular motors such as kinesin and myosin-V, the approach usually used is the multi-state chemical kinetic description where it is postulated that a motor protein steps through a sequence of discrete chemical states [17]. Using this approach, some of the experimental results on the kinetic behaviors of myosin-V are well fitted [18].

In this paper, we present a new model based on our previous work [19] by incorporating the detailed nucleotide-state-dependent orientation of the neck domain relative to the motor domain. The model can explain well the recent experimental observations that two substeps occur in some 36-nm steps while no substeps occur in other 36-nm steps [11]. Based on the model and the multi-state chemical kinetic description, we develop a theoretical approach to study the kinetics of single myosin-V molecules, with theoretical results in good agreement with previous available experimental results [2,4,11].

* Corresponding author. Tel.: +86 10 82649568; fax: +86 10 82640224.
E-mail address: pxie@aphy.iphy.ac.cn (P. Xie).

0301-4622/$ - see front matter © 2005 Elsevier B.V. All rights reserved.
doi:10.1016/j.bpc.2005.11.008

2. Model

It is generally known that the interaction force between myosin and actin in an ATPase cycle depends on its nucleotide state: In ATP state myosin has negligible interaction with actin. In ADP.Pi state it has a weak interaction with actin. Upon release of Pi, i.e., in ADP state, and ensuing release of ADP, i.e., in nucleotide-free state, myosin becomes to have strong interactions with actin [20–23].

Furthermore, according to previous experimental results, the relative orientation of the neck domain with respect to the motor domain in the presence of actin is also dependent on its nucleotide state: In weak actin-bound state (ADP.Pi) the relative orientation is random [24–30], as schematically shown in Fig. 1 (a). This is also consistent with the recent experimental results, demonstrating that, when ADP.Pi myosin-V was mixed with actin, both heads simultaneously release Pi at the same rate as the single-headed myosin-V [12,31]. Due to the random orientation of the neck domain relative to the motor domain, both heads can bind weakly and stereo-specifically to actin and thus release Pi simultaneously. However, if the relative orientation is fixed, due to the weak binding force to actin, the two heads in ADP.Pi states could not bind simultaneously to actin in the same orientation and thus the Pi release of the two heads would not take place at the same time.

Upon Pi release the relative orientation is fixed, as schematically shown in Fig. 1(b). After transition from the initial ADP* (i.e., Actin.Myosin*.ADP) state to its isomerization ADP (i.e., Actin.Myosin.ADP) state, the neck domain rotates from pre-power-stroke orientation (Fig. 1(b)) to post-power-stroke orientation, as shown in Fig. 1(c) [20,21,25,31]. The overall conformation of the nucleotide-free state is taken nearly the same as that of ADP state [20,21,25,31], as shown in Fig. 1(d). It is noted that there has been no consensus on whether the power stroke takes place before, concomitantly with or after Pi release. Here we assume that the power stroke of myosin-V takes place after Pi release, as adopted in Refs. [20,21,25,31]. For certain types of myosin, it was shown that another power stroke may also occur after ADP release [32,33]. For simplicity and without loss of generality, we neglect this power stroke induced by ADP release.

For the wild-type dimeric myosin-V with both heads in nucleotide-free state in the absence of actin, from the conformation of its single-headed counterpart (Fig. 1(d)) it is reasonable to assume that the equilibrium conformation of the dimer should have the form as shown in Fig. 2(a), with the relative orientation of the two heads being nearly mirror symmetrical. This can also be understood as follows: As stated in Ref. [34], the two heads of a homodimeric molecular motor such as myosin-V emerge from a coiled coil of α-helices, each helix extending into a neck. Because the coiled coil is twofold symmetric, as confirmed for kinesin [35] and myosin [36], the two identical motor domains are also arranged, basically, in the same twofold symmetry, i.e., the two motor domains would be oriented in opposite directions.

It is argued here that the residue segment connecting the neck domain and the coiled coil behaves elastically, with a small non-zero torsional/bendable elastic stiffness, rather than as a completely flexible element of nearly zero torsional/bendable stiffness (i.e., the residue segment being a "hinge point" around which the neck domain can rotate freely). This is in agreement with the recent experimental result by using single-molecule nanomechanics method for myosin-II [37], where the bending stiffness of the "hinge points" or residue segments that connect the neck domains and the colied coils was estimated to be 2.5 k_BT/rad. Furthermore, based on this argument, the non-zero torsional/bendable stiffness of the "hinge points" or the residue segments would keep the two heads of myosin-V fluctuating, due to noise, around their equilibrium orientations in a limited range. This is also in agreement with the earlier experimental results by using phosphorescence anisotropy decay measurements for conventional myosin-II in Ref. [38]: myosin heads have a favored orientation with a relatively small angular range with semi-angle of about 12.5° under relaxing conditions. In addition, by using the same method Ishiwata et al. [39] have shown that a myosin-II in solution consists of two components of rotation in cones with semi-angles of about 32° and 47°, respectively. The former component was attributed to the rotation of the myosin head (the motor domain and the neck domain) relative to the tail [39]. *This means that the myosin head can only rotate "freely" around the "hinge point" or residue segment in a limited range of 32° semi-angle* (noting that the previous models require that a myosin-V head should freely rotate in a range of more than 120° in order for the detached trailing head to diffuse to the next binding site after ATP binding). However, if this "hinge point" or residue segment is a flexible element of nearly zero torsional/bendable stiffness, which means a free rotation of the myosin head around the "hinge point", it would be expected that the rotation of the myosin head to the tail should be in a wider range of up to 90° in semi-angle under the experimental condition in Ref. [39]. Due to the non-zero stiffness, the thermal noise induces the rotation

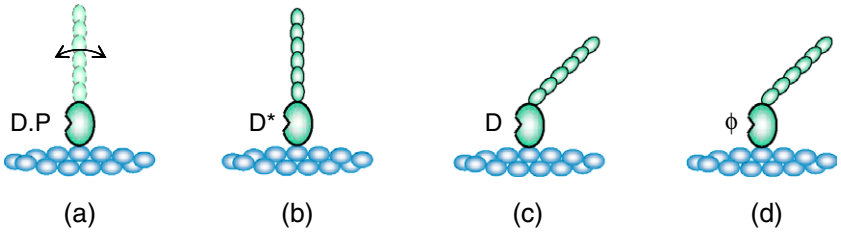

Fig. 1. Nucleotide-dependent relative orientation of the myosin neck domain with respect to its motor domain. The arrowed line in (a) indicates mobility. *T*, *D*, *P* and ϕ represent ATP, ADP, Pi and nucleotide-free, respectively.

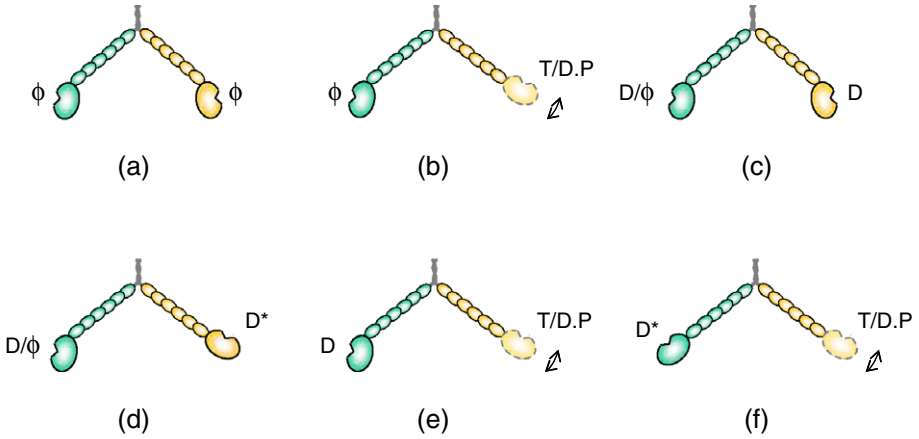

Fig. 2. Equilibrium conformations of dimeric myosin-V in different nucleotide states. The arrowed lines indicates mobility.

in the range with the semi-angle of only 32° around its equilibrium orientation. Thus, for myosin-V, it is similarly expected that the non-zero stiffness of the two "hinge points" or residue segments connecting the necks and the coiled coils would keep its two heads fluctuating in a limited range around their equilibrium orientations, as shown in Fig. 2. The favored orientations with a limited angular range for the two heads are also supported by various EM observations of myosin conformations in the absence of actin [40–42].

When ATP binds to one head, from Figs. 1(a) and 2(a) we deduce that the equilibrium conformation of the dimer has the form as shown in Fig. 2(b). After hydrolysis of ATP to ADP.Pi, the equilibrium conformation still shows the same form. Similarly, the equilibrium conformations of the dimer with its heads in other nucleotide states are schematically shown in Fig. 2(c)–(f). As in the case of kinesin [43], the motor domains of myosin V should also bind to actin in a fixed orientation, as shown in Fig. 1, i.e., the interaction between the motor domains and actin is stereospecific.

Since each head of myosin-V has a long neck domain, containing 6 IQ motifs plus 6 light chains, the long neck domain can be bended elastically [44]. Thus when the two heads are in ADP/nucleotide-free state or when one head in ADP/nucleotide-free state and the other one in ADP* state, the two heads can simultaneously bind strongly to two successive binding sites on actin in equivalent orientations which are schematically shown in Fig. 3(a) and (b). For the right head to bind actin in these conformations, an internal elastic force resulted mainly from the bending of the neck domains and a small internal torque resulted mainly from the torsion of the residue segment connecting the neck domain and the coiled coil should be overcome. When one head in ADP/nucleotide-free state and the other one in ADP.Pi state, the former head binds strongly to one binding site on actin and the other one can bind weakly to the successive binding site by overcoming now only the small internal torque resulted from the torsion of the residue segment connecting the neck domain and the coiled coil, as shown in Fig. 3(c). Note that the neck shapes in Fig. 3(a) and (b), which are determined by the internal elastic force and torque resulted from the change in the orientation of the right head from its equilibrium orientations as shown in Fig. 2(c) and (d), are consistent with the electron-microscopy observations either in the presence of ATP or in the absence of ATP or ADP [45]. The neck shapes in Fig. 3(c) were also observed [45]. Once one of the two heads or both become free, the internal elastic force and torque drives the dimeric myosin to its equilibrium (i.e., the minimum-free-energy) state (Fig. 2).

The proposed model is described as follows. We begin with the two heads in nucleotide-free states bound strongly to two successive binding sites on actin, as shown in Fig. 4(a) or Fig. 5 (a). According to the moving direction, we will call the head close to the barbed end (right) the leading head and that close to the pointed end (left) the trailing head. Since, in Fig. 4(a), ATP can either bind to the trailing head earlier than to the leading head or bind to the leading head earlier than to the trailing head, we consider the two cases, (i) ATP binds to the trailing head earlier and (ii) ATP binds to the leading head earlier, separately.

2.1. ATP binds to the trailing head (Fig. 4(a))

The interaction force of the trailing head with actin becomes smaller than the internal elastic force. Thus the trailing head is driven to its equilibrium position, the trailing head becoming the

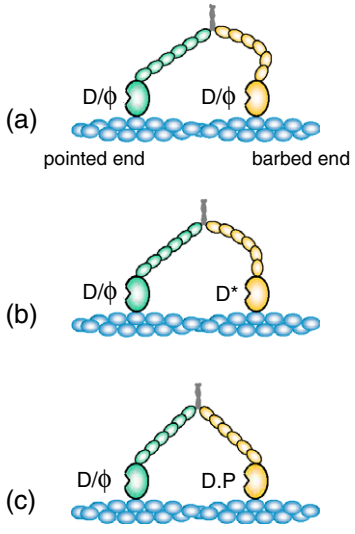

Fig. 3. Myosin-V binds, with both heads, to actin in different nucleotide states.

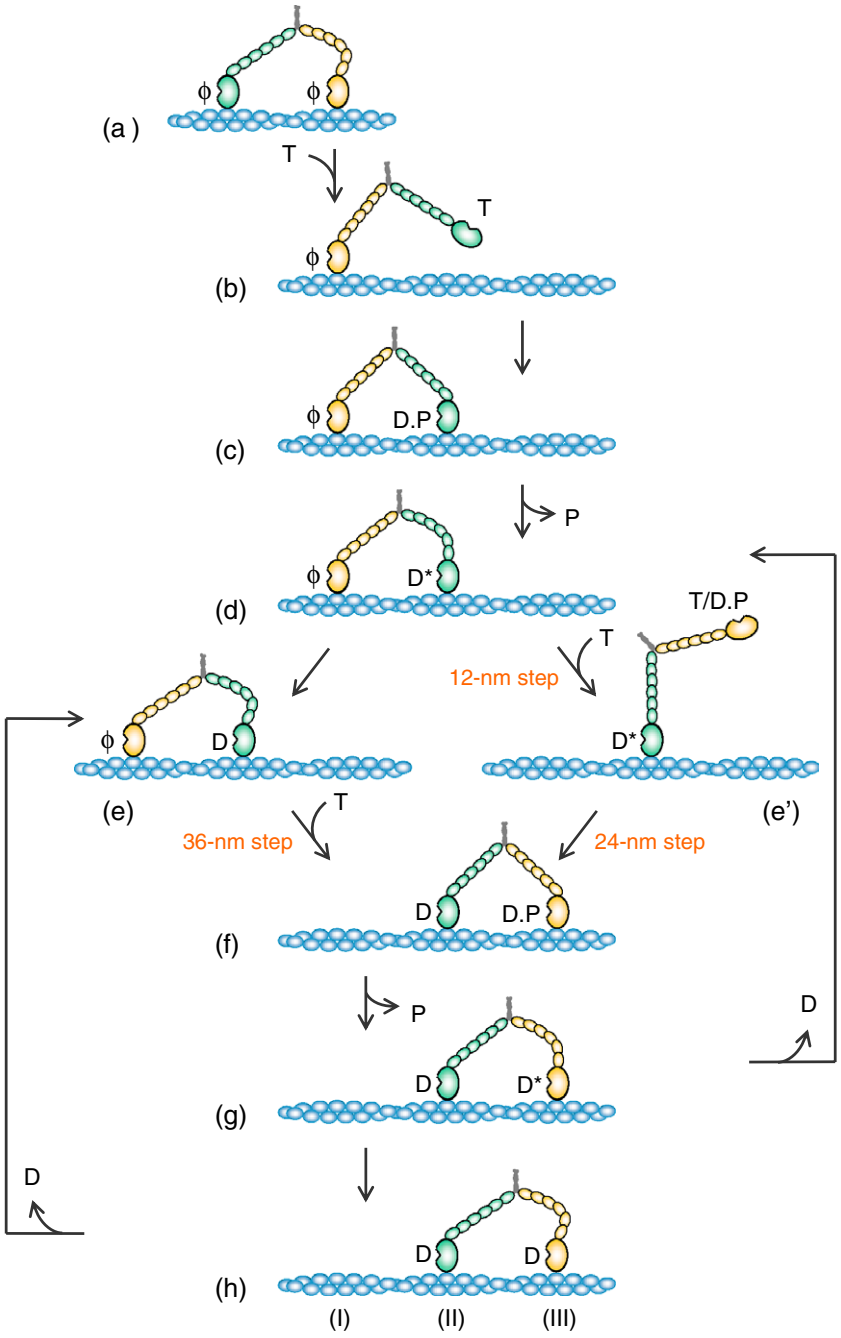

Fig. 4. Schematic illustrations of proposed movement mechanism of myosin-V with effective mechanochemical couplings. The intermediate *D′* state before ADP release is, for simplicity, not shown.

new leading head (Fig. 4(b)). Due to the very high ATP-hydrolysis rate, ATP is hydrolyzed to ADP.Pi immediately. Now the new leading head in ADP.Pi state binds weakly to actin [binding site (II)] near its equilibrium position, as shown in Fig. 4(c). Activated by actin, Pi is released immediately and the leading head, now in ADP* state, becomes bound strongly to site (II) and its neck domain is fixed, as shown in Fig. 4(d). Note that, due to the much high ATP hydrolysis rate (~750 s^{-1}) and actin-activated Pi release rate (>250 s^{-1}) [3], in Fig. 4(b) and (c) the probability of ATP binding to the new trailing head (yellow) is extremely low. (If ATP binds to the new trailing head in Fig. 4 (b) and (c), due to the weak binding force of the new leading head in ATP/ADP.Pi state, myosin-V is most probable to detach from actin.).

In Fig. 4(d), if the leading head changes from ADP* state to the intermediate isomerization ADP state before ATP binding to the trailing head, the neck domain of the leading head rotates in the clockwise direction, as shown in Fig. 4(e). Then upon ATP binding to the trailing head, the trailing head is driven to its equilibrium position, becoming the new leading head. After ATP hydrolysis, the new leading head binds weakly to actin [binding site (III)] near its equilibrium

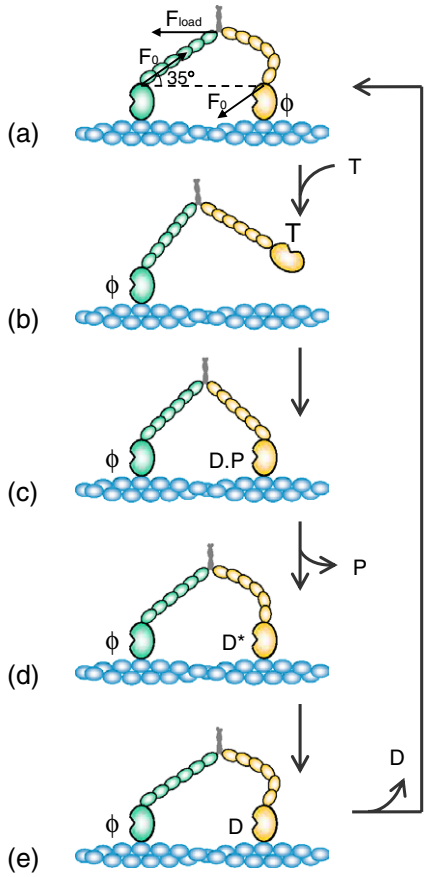

Fig. 5. Schematic illustrations of the movement of myosin-V with a futile mechanochemical coupling.

position, as shown in Fig. 4(f). Activated by actin, Pi is released immediately and the leading head, now in ADP* state, becomes bound strongly to site (III) and its neck domain is fixed, as shown in Fig. 4(g). Note again that, due to the much higher actin-activated Pi release rate (>250 s^{-1}) than ADP release rate (~12 s^{-1}) [3], the probability of ADP release from the new trailing head (green) is negligibly low in Fig. 4(f). From Fig. 4(g), if ADP release from the trailing head proceeds the ADP* to ADP transition of the leading head, myosin-V returns to the state of Fig. 4(d), with the motor moved one step toward the barbed end. From Fig. 4(d), through (e), (f) and (g), to (d), an effective mechanochemical cycle is completed. On the contrary, from Fig. 4(g), if the ADP* to ADP transition of the leading head proceeds ADP release from the trailing head, myosin-V will complete one effective mechanochemical cycle from Fig. 4(e), through (f), (g) and (h), to (e). In either of the two cases no substeps occur. This is consistent with the recent experimental result that, in some 36-nm steps, no substep could be identified even at a 10-kHz sampling rate [11].

In Fig. 4(d), if ATP binding to the trailing head occurs before the leading head changes from ADP* to ADP states, the trailing head is driven to its equilibrium position, becoming the new leading head, as shown in Fig. 4(e′). Since Pi cannot be released without activation of actin in this situation, the new leading head will remain in ADP.Pi state. Then as the neck domain of the new trailing head rotates clockwise following state transition from ADP* to ADP, the new leading head can bind weakly to actin near binding site (III), as shown in Fig. 4(f). Activated by actin, Pi is released and the leading head, now in ADP* state, becomes bound strongly to site (III), as shown in Fig. 4(g). After ADP is released from the trailing head, myosin-V returns to the state of Fig. 4(d), with the motor moved one step toward the barbed end. From Fig. 4(d), through (e′), (f) and (g), to (d), an effective mechanochemical cycle is completed, in which there exist two substeps, with one substep from Fig. 4(d) to (e′) and the other one from Fig. 4(e′), through (f) and (g), to (d). From previous experiments, it is known that the power-stoke size is ~25 nm [6], which means that the size of the second substep is ~25 nm and thus the size of the first substep should be ~11 nm (the average step size 36 nm minus 25 nm). This is in agreement with the recent experimental result that some 36-nm steps consist of two consecutive substeps of 12 and 24 nm [11].

2.2. ATP binds to the leading head (Fig. 5(a))

The leading head is driven by internal elastic force and torque to its equilibrium position (Fig. 5(b)). Then ATP is hydrolyzed to ADP.Pi immediately. Now the leading head binds weakly to actin (Fig. 5(c)). Upon Pi release, the leading head becomes bound strongly to actin and its neck linker is fixed, as shown in Fig. 5(d). The leading head changes from ADP* to ADP states (Fig. 5(e)) and then ADP is released, thus myosin-V returning to the original state in Fig. 5(a). A futile mechanochemical cycle is completed.

In fact, when the two heads of myosin-V simultaneously bind strongly to actin, there exists a forward internal elastic force on the trailing head and a backward force on the leading head. As will be discussed in Section 4, this leads to a much high ADP-release rate of the trailing head compared with that of the leading head. That is, it rarely occurs that the leading head is in nucleotide-free state. Therefore, the futile mechanochemical cycle rarely occurs and myosin-V generally hydrolyzes one ATP per step (1 : 1 mechanochemical coupling).

3. Theoretical approach

As noted above, the ATPase cycling of a given myosin head is described by, $\mathrm{ADP^*} \underset{k_{-1}}{\overset{k_1}{\rightleftharpoons}} \mathrm{ADP} \underset{k_{-2}}{\overset{k_2}{\rightleftharpoons}} \mathrm{ADP'} \underset{k_{-3}}{\overset{k_3}{\rightleftharpoons}} \mathrm{Empty} \underset{k_{-4}}{\overset{k_4}{\rightleftharpoons}} \mathrm{ATP} \underset{k_{-5}}{\overset{k_5}{\rightleftharpoons}} \mathrm{ADP.Pi} \underset{k_{-6}}{\overset{k_6}{\rightleftharpoons}} \mathrm{ADP^*}$, where besides the intermediate ADP state as discussed in Section 2, it is assumed that there also exists another intermediate state for ADP release [22,23,31,46,47], denoted by ADP′, which has the same conformation as ADP state. Though this ATPase pathway should be general for all members of the myosin superfamily, different classes of myosins have different reaction rates and thus different rate-limiting steps and duty ratios for adaptations to different functions [12,23]. For myosin-V, due to the much high ATP hydrolysis rate, $k_5 \approx 750\ s^{-1}$, compared with other rates [3], it is a very good approximation that we neglect the time taken for ATP hydrolysis during one ATPase cycle. Thus in

one ATPase cycle of a myosin-V head we need only to consider the following scheme

$$\mathrm{ADP^{*}} \xrightarrow{k_1} \mathrm{ADP} \xrightarrow{k_2} \mathrm{ADP'} \underset{k_{-3}}{\overset{k_3}{\rightleftarrows}} \mathrm{Empty} \xrightarrow{k_4} \mathrm{ATP/ADP.Pi} \xrightarrow{k_6} \mathrm{ADP^{*}}, \tag{1}$$

where, for simplicity, we have neglected the transition from ADP′ to ADP as the ADP concentration is assumed low here, and neglected the much slow transition from ATP state to Empty (i.e., nucleotide-free) state. The transition rates k_i (i=1, 2, 3, 6) are independent of [ATP] and [ADP], k_4 is [ATP] dependent, i.e., $k_4=k_T$ [ATP] and k_{-3} is [ADP] dependent, i.e., $k_{-3}=k_D$ [ADP]. Since the actin-activated Pi release rate, $k_6>250\ s^{-1}$, is much larger than k_i (i=1, 2, 3) [3], the time for Pi release from Fig. 4(f) to (g) can be negligible. Without the activation of actin in Fig. 4(e′), the Pi release rate $k_6\approx 0$.

When a force parallel with the moving direction, F, is acted on a myosin head, the dependence of chemical reaction rates on F follows the kinetics of an enzymatic reaction, which is in the general Boltzmann form [48]

$$k_i = \frac{k_{i0}(1+A_i)}{1+A_i\exp(F\delta_i/k_BT)} \quad (i=1,2,3,T,D), \tag{2a}$$

where $k_i=k_{i0}$ is load independent when $A_i=0$. F is defined as positive when it is opposite to the moving direction. When a force perpendicular to the moving direction, $F^{(\perp)}$, is acted on the myosin head, the chemical reaction rates have the same Boltzmann form as that of Eq. (2a) but with $F^{(\perp)}$, $A_i^{(\perp)}$ and $\delta_i^{(\perp)}$ instead of F, A_i and $\delta_i^{(\perp)}$. $F^{(\perp)}$ is defined as positive when it is helpful to detach the myosin from actin. When both forces, F and $F^{(\perp)}$, are acted simultaneously on the head, the chemical reaction rates become

$$k_i = \frac{k_{i0}[1+A_i][1+A_i^{(\perp)}]}{[1+A_i\exp(F\delta_i/k_BT)][1+A_i^{(\perp)}\exp(F^{(\perp)}\delta_i^{(\perp)}/k_BT)]}. \tag{2b}$$

When substeps occur, the main dwell time, defined as the time interval following the 24-nm substepping in Ref. [11], corresponds to the period from Fig. 4(f), through (g) and (d), to (e′). Thus from Scheme (1) the main dwell time corresponds to the following scheme for the head that is trailing in Fig. 4(f)

$$\mathrm{ADP} \xrightarrow{k_2} \mathrm{ADP'} \underset{k_{-3}}{\overset{k_3}{\rightleftarrows}} \mathrm{Empty} \xrightarrow{k_4} \mathrm{ATP}. \tag{3}$$

When substeps do not occur the main dwell time corresponds to the period either from Fig. 4(f), through (g), (d) and (e), to (f) or from Fig. 4(f), through (g), (h) and (e), to (f). For the former case, Scheme (3) describes the states of the head that is leading in Fig. 4(e) and then becomes trailing in Fig. 4(f), (g), (d) and (e). As we will see in Section 4, the ADP-release rate of the leading head is much lower than that of the trailing head. Thus, to a very good approximation, we can neglect the transition from ADP to ADP′ states of the leading head in Fig. 4(e) and thus the main dwell time can be calculated by using Scheme (3) for the *trailing* head. For the latter case, Scheme (3) describes the states of the head that is leading in Fig. 4(h) and (e) and then becomes trailing in Fig. 4(f), (g), (h) and (e). As discussed in the former case, to a very good approximation, we can neglect the transition from ADP to ADP′ states of the leading head in Fig. 4 (h) and (e) and the main dwell time can still be calculated by using Scheme (3) for the *trailing* head.

In rigor state of Figs. 4(a) or 5(a), the force opposite to the moving direction acted on the trailing head can be written as

$$F = F_{\mathrm{load}} - F_0\cos 35°, \tag{4a}$$

and that acted on the leading head can be written as

$$F = F_{\mathrm{load}} + F_0\cos 35°, \tag{4b}$$

where F_0 is the internal elastic force. The force perpendicular to the moving direction acted on the trailing and leading heads are, respectively,

$$F^{(\perp)} = F_0\sin 35°, \tag{4c}$$

$$F^{(\perp)} = -F_0\sin 35°. \tag{4d}$$

In calculations we take the internal elastic force in the moving direction equal to the stall force, i.e., $F_0\cos 35°=3$ pN [2]. This is because, when a load equal to $F_0\cos 35°$ is acted on the myosin, the net force acted on the trailing head F in the moving direction is zero (see Eq. (5a)) and thus the motor becomes stalled since the trailing head on average cannot move either forward or backward even if it is detached from actin after ATP binding.

Now we derive the formula for the main dwell time distribution. For convenience of writing, we denote the probabilities for finding the fixed myosin head in ADP, ADP′, Empty, and ATP states by D, D', ϕ, and T, respectively. From scheme (3), the probabilities are described by the following differential equations

$$dD/dt = -k_2D, \tag{5a}$$

$$dD'/dt = k_2D + k_{-3}\phi - k_3D', \tag{5b}$$

$$d\phi/dt = k_3D' - (k_{-3}+k_4)\phi, \tag{5c}$$

$$dT/dt = k_4\phi, \tag{5d}$$

where F and $F^{(\perp)}$ used for calculating k_i are given by Eqs. (4a) and (4c). Solving Eqs. (5a)–(5d) with the initial conditions $D(0)=1$, $D'(0)=0$, $\phi(0)=0$ and $T(0)=0$, we obtain the probability density for the main dwell time, $f_M(t)=dT/dt$, as follows

$$f_M(t) = \frac{k_2k_3k_4}{2b}\left(\frac{e^{(a+b)t}}{k_2+a+b} - \frac{e^{(a-b)t}}{k_2+a-b} + \frac{2be^{-k_2t}}{(k_2+a+b)(k_2+a-b)}\right), \tag{6}$$

Table 1
Values of parameters used for fitting experimental results in Refs. [2] and [4]

i	k_{i0}	A_i	$A_i^{(\perp)}$	$\delta_i(\delta_i^{(\perp)})$
2	12 s^{-1}	0	0	
3	24.3 s^{-1}	717	1	12 nm
T	1.21 $\mu M^{-1} s^{-1}$	0	0	

where $a=-(k_3+k_{-3}+k_4)/2$ and $b=(a^2-k_3k_4)^{1/2}$. From Eq. (6), the average main dwell time is

$$\tau_M = k_2^{-1} + k_3^{-1} + k_4^{-1} + k_{-3}k_3^{-1}k_4^{-1}. \quad (7)$$

In the case of no ADP, τ can be written as

$$\tau_M = \frac{k_{23}/k_T + [ATP]}{k_{23}[ATP]}, \quad (8)$$

where $k_{23}=k_2k_3/(k_2+k_3)$ is the average ADP-release rate. Note that Eq. (8) has the Michaelis–Menten form.

Next, we study the intermediate dwell time distribution. As can be noted from our model, the intermediate dwell time corresponds to the time taken by myosin head to change from ADP* state in Fig. 4(e′) to ADP state in Fig. 4(f). This time is only part of the ADP* to ADP transition time of the head that is leading in Fig. 4(g) and (d) and then becomes trailing in Fig. 4(e′). We first determine the distribution of the overall time taken by this myosin head to change from ADP* to ADP states (from Fig. 4(g), through (d) and (e′), to (f)), which is described by the scheme, ADP* $\xrightarrow{k_1}$ADP. From this scheme the probabilities for finding this head in ADP* and ADP states are described by the following differential equations

$$dD^*/dt = -k_1D^*, \quad (9a)$$

$$dD/dt = k_1D^*, \quad (9b)$$

where the forces for calculating k_1 are given by Eqs. (4b) and (4d) when the ADP*-head is leading (Fig. 4(g) and (d)), whereas the forces for k_1 are simply $F\approx F_{load}$ and $F^{(\perp)}=0$ when the ADP*-head is trailing (Fig. 4(e′)). Solving Eqs. (9a) and (9b), with the initial conditions $D^*(0)=1$ and $D(0)=0$, we obtain the probability density for the time of ADP* to ADP transition as $g(t)=k_1e^{-k_1t}$, which is a single-exponential form. The distribution of the intermediate dwell time thus should also have a single-exponential form

$$f_I(t) = k_Ie^{-k_It}, \quad (10)$$

where $k_I=1/\tau_I$, with τ_I being the average intermediate dwell time.

As the intermediate state occurs, myosin changes its conformation via two periods during the ADP* to ADP transition, one from Fig. 4(g), through (d), to (e′), and the other from Fig. 4(e′) to (f). Thus we have the relation

$$k_1^{(L)}\Delta t + k_1^{(T)}\tau_I = 1, \quad (11)$$

where $k_1^{(L)}$ is the ADP* to ADP transition rate when myosin head is leading with $F\approx F_{load}+F_0\cos 35°$ and $F^{(\perp)}=-F_0\sin 35°$, as shown in Fig. 4(g) and (d), and $k_1^{(T)}$ is that when the head is trailing with $F=F_{load}$ and $F^{(\perp)}=0$, as shown in Fig. 4(e′). Δt is the average time taken by the myosin to change its conformations from Fig. 4(g), through (d), to (e′) and τ_I the average time taken by the myosin to change its conformation from Fig. 4(e′) to (f), i.e., the average intermediate dwell time. From Eq. (11) we have

$$\tau_I = \frac{1-k_1^{(L)}\Delta t}{k_1^{(T)}}. \quad (12)$$

Considering that the occurrence frequency of the intermediate state is around 0.5 for the case of saturating [ATP], no ADP and no BDM [11], as an approximation, we can take Δt equal to half of the time taken by the trailing head to change from ADP state to nucleotide-free state under the conditions of *saturating* [ATP], no ADP and no BDM, i.e., $\Delta t=(k_2^{-1}+k_3^{-1})/2$, with $F=F_{load}-F_0\cos 35°$ and $F^{(\perp)}=F_0\sin 35°$ in calculations of k_2 and k_3.

The occurrence frequency, P_I, of the intermediate state corresponds to the probability that the release of ADP from and then ATP binding to the *trailing* head (from Fig. 4(f), through (g) and (d), to (e′)) are completed earlier than the change from ADP.Pi to ADP* and then to ADP of the *leading* head (either from Fig. 4(f), through (g) and (d), to (e) or from Fig. 4(f), through (g), to (h)). The time distribution of the former process is calculated by using Eqs. 4(a) (c) and (6), while the time distribution of the latter process is calculated by using $g(t)=k_1e^{-k_1t}$ with $F\approx F_{load}+F_0\cos 35°$ and $F^{(\perp)}=-F_0\sin 35°$ in calculations of k_1 (Note that Pi release time is negligible). As an approximation, P_I can be calculated by the following equation

$$P_I = \frac{\tau_M^{-1}}{\tau_M^{-1}+k_1}, \quad (13)$$

with $F=F_{load}-F_0\cos 35°$ and $F^{(\perp)}=F_0\sin 35°$ in calculations of τ_M and $F\approx F_{load}+F_0\cos 35°$ and $F^{(\perp)}=-F_0\sin 35°$ in calculations of k_1.

4. Results

The values of parameters are shown in Tables 1 and 2, where Table 1 is for fitting the experimental results in Refs. [2] and [4] and Table 2 is for fitting the experimental results in Ref. [11]. We see that the corresponding values in the two tables are close. From Table 1 we obtain, under zero force acted on a single

Table 2
Values of parameters used for fitting experimental results in Ref. [11]

i	k_{i0}	A_i	$A_i^{(\perp)}$	$\delta_i(\delta_i^{(\perp)})$
1	45.45 s^{-1}	3×10^{-8}	0	16.55 nm
2	15 s^{-1}	0	0	
3	13.6 s^{-1}	1611	1	13 nm
T	0.222 $\mu M^{-1} s^{-1}$	0	0	
D	9.324 $\mu M^{-1} s^{-1}$	0	0	

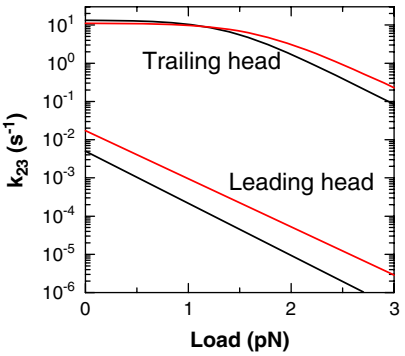

Fig. 6. The calculated ADP-release rate, k_{23}, of the trailing head and that of the leading head in rigor state with both heads bound strongly to actin. Black lines are calculated by using parameters given in Table 1 and red lines using parameters given in Table 2. (For interpretation of the references to colour in this figure legend, the reader is referred to the web version of this article.)

myosin head, the ATP-binding rate k_T=1.21 μM^{-1} s^{-1} and the ADP-release rate $k_{D\text{-release}}$=9.7 s^{-1}. From Table 2 we obtain the ATP-binding rate k_T=0.222 μM^{-1} s^{-1}, the ADP-binding rate k_D=9.324 μM^{-1} s^{-1}, and the ADP-release rate $k_{D\text{-release}}$=8.3 s^{-1} under zero force. These values are consistent with the corresponding experimental values for a monomer, with ATP-binding rate of 0.9 μM^{-1} s^{-1}, ADP-binding rate of 12.6 μM^{-1} s^{-1} and ADP-release rate of 12 s^{-1} [3]. Using the parameters given in Tables 1 and 2 we calculate ADP-release rate, k_{23}, of the trailing head and that of the leading head in rigor state with both heads bound strongly to actin. The calculated results are shown in Fig. 6. From Fig. 6 it is seen that k_{23} of the trailing head is much larger than that of the leading head, which means that ADP release from the leading head rarely occurs. This is in agreement with the experimental observations [12].

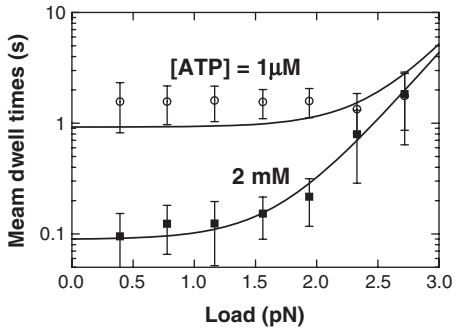

Fig. 8. Dependences of mean dwell time on load at different [ATP]. Solid lines are calculated results and data points are taken from Ref. [2].

First, using parameters given in Table 1 we make calculations and comparisons with the experimental results in Refs. [2] and [4]. Using Eq. (6) the calculated main dwell-time distributions for various ATP concentrations and no ADP under low load (<1 pN), where the dwell time is unaffected by load, are shown in Fig. 7(a)–(c). The theoretical results are in good agreement with the experimental ones [4]. As did in Ref. [4], we verified that the distributions can be fitted very well by using the two-exponential form,

$$f'(t) = \frac{k_1' k_2'}{k_2' - k_1'}[\exp(-k_1' t) - \exp(-k_2' t)]. \quad (14)$$

If, as did in Ref. [4], we fix $k_1'=k_2$=12 s^{-1}, the fitted values of k_2' as a function of [ATP] are shown in Fig. 7(d) (rhombus points), where triangular and square points are the experimental results [4]. We see that the fitted values of k_2' are in good agreement with the experimental ones. It is interesting to note

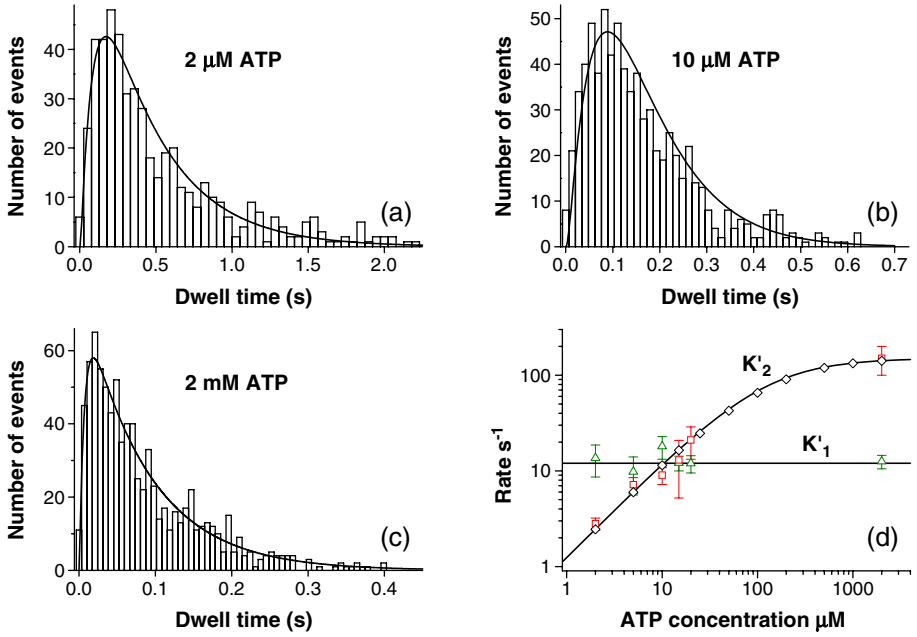

Fig. 7. The main dwell time distributions at (a) [ATP]=2 μM, (b) [ATP]=10 μM, (c) [ATP]=2 mM. The solid lines are theoretical results and the columns are experimental results taken from Ref. [4]. (d) k_1' and k_2' as a function of [ATP]. Rhombuses are fitted values of k_2' (with k_1' fixed at 12 s^{-1}) and the solid line is calculated from Eq. (15). Triangles (green) and squares (red) are experimental results taken from Ref. [4]. (For interpretation of the references to colour in this figure legend, the reader is referred to the web version of this article.)

that k_2' versus [ATP] follows very well the Michaelis–Menten equation,

$$k_2' = \frac{k_3[\mathrm{ATP}]}{k_3/k_T + [\mathrm{ATP}]}, \tag{15}$$

as shown by line in Fig. 7(d). This is understood as follows: At saturating [ATP], k_2' becomes the same as k_3 and the [ATP] dependence of k_2' is only through the ATP binding. In fact, from Eq. (14), the mean dwell time can be obtained as $\tau = 1/k_1' + 1/k_2'$. By comparing it with Eq. (8), we see that, if we let $k_1' = k_2$, then we obtain Eq. (15).

Using Eq. (8) we calculate the average main dwell time versus load, with the results shown in Fig. 8. Note that, although the experimental results as shown in Figs. 7 and 8 are obtained from different experiments [2,4], the theoretical results using one set of parameter values show good agreement with all these experimental results.

Second, using parameters given in Table 2 we make calculations and comparisons with the experimental results in Ref. [11]. Using Eq. (7) we give the calculated average main dwell time versus load at various nucleotide states in Fig. 9(a). For the effect of BDM [11], we assume that it only affects the values of k_{10}, A_1 and k_{20}, i.e., $k_{10} = 12.5\ \mathrm{s}^{-1}$, $A_1 = 1 \times 10^{-7}$ and $k_{20} = 9.1\ \mathrm{s}^{-1}$ and it has no effect on the other parameters. From Eqs. (10) and (12), we note that both the intermediate dwell time distribution and the average intermediate dwell time are independent of the concentrations of ATP and ADP, which is consistent with the experimental results [11]. Using Eq. (12) we give the calculated average intermediate dwell time versus load in Fig. 9(b). Using Eqs. (6) and (10) the calculated main dwell time distribution and intermediate dwell time distribution are

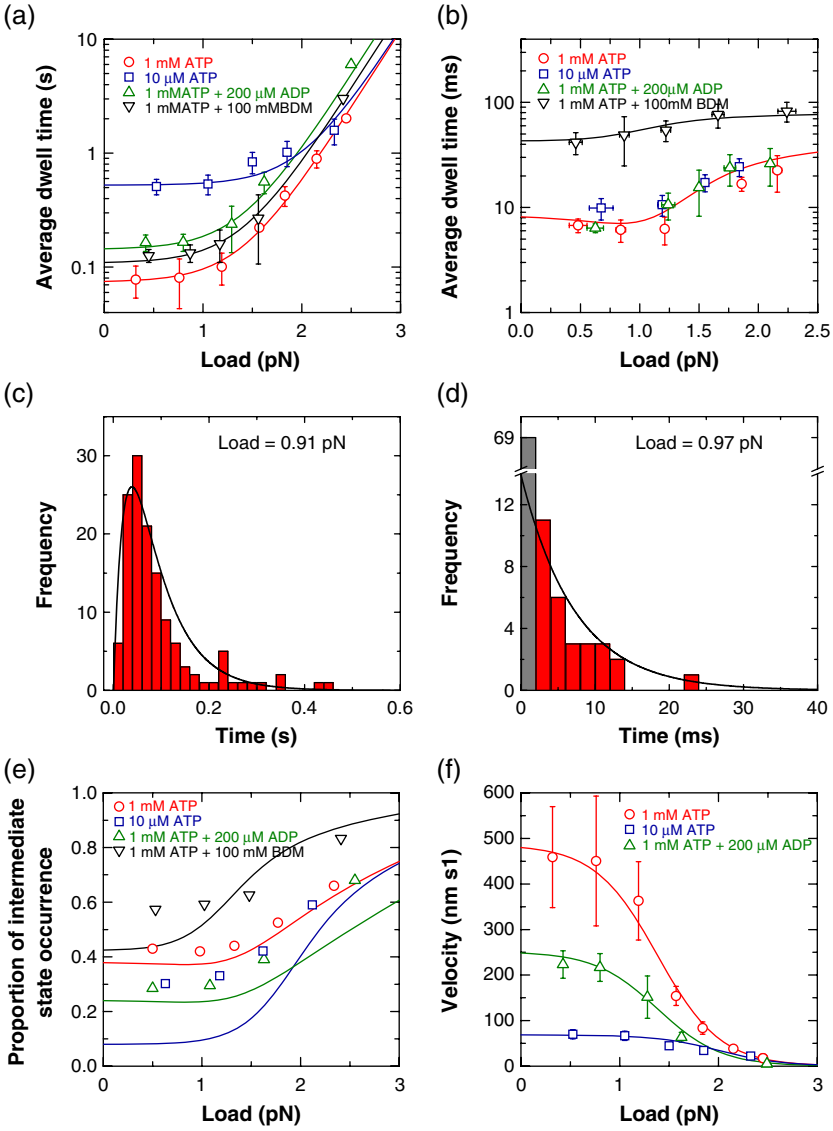

Fig. 9. Load dependence of the main and the intermediate dwell times at various nucleotide states, of the occurrence frequency of the intermediate state, and of the moving velocity. Solid lines are calculated results and data points (or columns) are experimental results [11]. (a) The average main dwell time versus load. (b) The average intermediate dwell time versus load. (c) The main dwell time distribution at load of 0.91 pN. (d) The intermediate dwell time distribution at load of 0.97 pN. (e) The occurrence frequency of the intermediate state versus load. (f) Load-velocity relationship.

shown in Fig. 9(c) and (d), respectively. Using Eq. (13) we show the calculated occurrence frequency of the intermediate state in Fig. 9(e). The average velocity is calculated by using equation, $V \approx 36/\tau_M$ (nm/s), with the results given in Fig. 9(f). It is seen from Fig. 9 that the calculated results show good agreement with the experimental results [11], except for the load dependence of occurrence frequency of the intermediate state (Fig. 9(e)). In the case of Fig. 9(e) the shapes of the theoretical curves still resemble the experimental results well. One of the possible reasons for the discrepancies between the calculated and experimental values is that the experimental results cannot be measured directly and are only estimated indirectly [11].

5. Discussion

Different experiments have consentaneously determined that myosin-V walks processively by generally consuming one ATP to make a step of ~36 nm. Most of the previous models made a taken-it-for-granted assumption of tight coordination between the two heads of myosin-V to analyze its processivity [4–6,8–12,14] and to calculate its kinetics [18]. Recently, by using elastic lever arm models [15,16], the coordination was explained by showing that the leading head only binds to actin after the power stroke in the trailing head and that it only undergoes its power stroke after the trailing head detaches from actin. In this work, we gave another explanation to this coordination: The results from the present model show that myosin-V walks along actin by generally consuming one ATP per step, which is due to much higher ADP-release rate of the trailing head than that of the leading head. The different ADP-release rates of the two heads, which are resulted from the different internal forces acted on the two head domains, ensure that myosin-V walks processively along actin for a long distance. Moreover, our model shows that the leading head undergoes its power stroke sometimes before the unbinding of the trailing head and sometimes after the unbinding of the trailing head. Thus our model is compatible with the currently prevailing hypothesis that the leading head undergoes it power stroke immediately after binding, thereby storing energy into elastic deformation of its lever arm and releasing it after the unbinding of the trailing head. It is also compatible with another hypothesis that the release of the trailing head is necessary for the power stroke in the leading head [16].

In previous models, Brownian motion plays an important role in the stepping of myosin-V. Experimental results show that the power stroke size, i.e., the distance of the lever arm tip movement between post-power-stroke state and pre-power-stroke state is ~25 nm, which is less than the measured mean movement distance, ~72 nm, of the detached motor domain [9]. Thus the next ~47 nm movement of the detached motor domain to the next binding site is presumed to be resulted from the Brownian motion. Note that it is implicitly assumed there that the residue segment connecting the neck domain and the coiled coil is a flexible element with zero torsional/bendable stiffness. In our present model, however, the Brownian motion is not important and the forward movement of the detached trailing head is mainly due to the internal force and torque that are induced by the deviation of the dimer's conformation from its equilibrium form. The site on actin where the detached leading head will bind is determined by both the equilibrium position of the detached leading head and the azimuthal angle of the binding sites on actin, which gives a mean movement distance of ~72 nm for the detached motor domain. Furthermore, because the distance between the two motor domains can only vary within a narrow range of Gaussian distribution around their equilibrium distance due to the Langevin noise, it is expected that the distribution of the movement distance of the detached motor domain, which is the convolution of the Gaussian position distribution of the detached motor domain and the distribution of the azimuthal-angle-dependent binding probability, will be narrow. This is consistent with the experimental results [4,9]. In addition, from the equilibrium distance between the two motor domains we expect that the distance between the two binding motor domains in nucleotide-free (i.e., post-power-stroke) states will also show a narrow range peaked at ~36 nm, similar to that observed during the working condition [4,45]. This is consistent with the electron microscopy observation in the absence of ATP or ADP [45]. Note that, if the residue segment connecting the neck domain and the coiled coil is a flexible element as assumed in previous models, the distribution of the distances between the two binding heads in nucleotide-free (or post-power-stroke) states should peak at a value much smaller than 36 nm, as calculated in Ref. [16]. This is obviously inconsistent with the electron microscopy observation by Walker et al. [45]. This gives another evidence for our argument of small non-zero torsional/bendable stiffness for the residue segments that connect the neck domains and the colied coils.

Experimental results show that, under high backward load, backward stepping is frequently observed [2,4]. Using our model this can be readily explained as follows: When ATP binds to the leading head (see, for example, Fig. 5(b)), the large backward load together with the Langevin force can overcome the internal elasticity to drive the lever arm of the trailing head bending backward and thus make the detached head bind to the previous binding site on actin and then release Pi. Thus a backward step is made. Recently, an interesting experiment on kinesin shows that, under very high backward loads larger than the stall force, the kinesin can walk backwards stepwisely and processively in an ATP-dependent manner [49]. Using our model, we expect that myosin-V can also have similar processive backward stepping. This can be understood as follows: For the case of a backward load larger than the stall force ($F_{stall}=F_0 \cos 35°$), even if an ATP binds to the trailing head, the detached trailing head cannot move forward to become the leading head due to the net backward force (i.e., $F=F_{load}-F_0 \cos 35°>0$) acted on the detached trailing head. On the other hand, when an ATP binds to the leading head, the myosin can move a backward step. Therefore, the myosin can move backwards stepwisely and processively. Since the ADP-release rate of the leading head is much smaller than the trailing head, during the dwell period between two successive backward stepping, the processes of ADP release is almost always completed in the trailing head, while the process of ATP binding usually starts in the trailing head and is sometimes completed

when it becomes the leading head. Since ATP binding is involved, the dwell time of the processive backward stepping is thus ATP dependent. Also, the ATP turnover is involved during the processive backward stepping. It should be interesting to verify this prediction in future experiments.

In addition, from Fig. 4(e′) we note that, at very high loads, the detached leading head is liable to bind the previous binding site. This is consistent with the experimental observation that "half steps" are always followed by another half step in either forward or backward direction [4]. Also, it is obvious that, because only one head is attached to action, the intermediate levels exhibit increased variance of fluctuation [4].

Several recent experiments on kinesins show that a kinesin homodimer walks along microtubule in a limping manner [50,51]. In other words, the mean dwell time values of two successive steps are different. However, using our present model we predict that myosin-V homodimer should not exhibit the similar limping behaviors. As shown in Fig. 4, in the equilibrium state (Fig. 4(b) or (e′)) the internal elastic force and torque are zero. After Pi release, as the leading head make a 180°-rotation in order to bind strongly to actin, it will take equal probability to rotate along the two opposite directions. Thus even the sideway force (perpendicular to the paper plane), which is resulted from the internal torque, has strong asymmetric effect on the ATPase rate of the head, the mean dwell time will not show *strict* alternation. Therefore, we conclude that, different from kinesin homodimer, myosin-V homodimer does not exhibit limping behaviors.

In conclusion, we present a new hand-over-hand model for the processive movement of myosin-V along actin. Based on the model, the calculated results on various kinetic behaviors show good quantitative agreement with previous experimental results.

Acknowledgements

This work was supported by the National Natural Science Foundation of China.

References

[1] S.L. Reck-Peterson, D.W. Provance Jr., M.S. Mooseker, J.A. Mercer, Class V myosins, Biochim. Biophys. Acta 1496 (2000) 36–51.
[2] A.D. Mehta, R.S. Rock, M. Rief, J.A. Spudich, M.S. Mooseker, R.E. Cheney, Myosin-V is a processive actin-based motor, Nature 400 (1999) 590–593.
[3] E.M. De La Cruz, A.L. Wells, S.S. Rosenfeld, E.M. Ostap, H.L. Sweeney, The kinetic mechanism of myosin V, Proc. Natl. Acad. Sci. U. S. A. 96 (1999) 13726–13731.
[4] M. Rief, R.S. Rock, A.D. Mehta, M.S. Mooseker, R.E. Cheney, J.A. Spudich, Myosin-V stepping kinetics: a molecular model for processivity, Proc. Natl. Acad. Sci. U. S. A. 97 (2000) 9482–9486.
[5] S. Burgess, M. Walker, F. Wang, J.R. Sellers, H.D. White, P.J. Knight, J. Trinick, The prepower stroke conformation of myosin V, J. Cell Biol. 159 (2002) 983–991.
[6] C. Veigel, F. Wang, M.L. Bartoo, J.R. Sellers, J.E. Molloy, The gated gait of the processive molecular motor, myosin V, Nat. Cell Biol. 4 (2002) 59–65.
[7] J.N. Forkey, M.E. Quinlan, M.A. Shaw, J.E. Corrie, Y.E. Goldman, Three dimensional structural dynamics of myosin V by single-molecule fluorescence polarization, Nature 422 (2003) 399–404.
[8] J.E. Molloy, C. Veigel, Myosin motors walk the walk, Science 300 (2003) 2045–2046.
[9] A. Yildiz, J.N. Forkey, S.A. McKinney, T. Ha, Y.E. Goldman, P.R. Selvin, Myosin V walks hand-over-hand: single fluorophore imaging with 1.5-nm localization, Science 300 (2003) 2061–2065.
[10] J.E. Baker, E.B. Krementsova, G.G. Kennedy, A. Armstrong, K.M. Trybus, D.M. Warshaw, Myosin V processivity: multiple kinetic pathways for head-to-head coordination, Proc. Natl. Acad. Sci. U. S. A. 101 (2004) 5542–5546.
[11] S. Uemura, H. Higuchi, A.O. Olivares, E.M. De La Cruz, S. Ishiwata, Mechanochemical coupling of two substeps in a single myosin V motor, Nat. Struct. Mol. Biol. 11 (2004) 877–883.
[12] S.S. Rosenfeld, H.L. Sweeney, A model of myosin V processivity, J. Biol. Chem. 279 (2004) 40100–40111.
[13] H.E. Huxley, The mechanism of muscular contraction, Science 164 (1969) 1356–1365.
[14] J.A. Spudich, R.S. Rock, A crossbridge too far, Nat. Cell Biol. 4 (2002) E8–E10.
[15] G. Lan, S.X. Sun, Dynamics of myosin-V processivity, Biophys. J. 88 (2005) 999–1008.
[16] A. Vilfan, Elastic lever arm model for myosin V, Biophys. J. 88 (2005) 3791–3805.
[17] M.E. Fisher, A.B. Kolomeisky, The force exerted by a molecular motor, Proc. Natl. Acad. Sci. U. S. A. 96 (1999) 6597–6602.
[18] A.B. Kolomeisky, M.E. Fisher, A simple kinetic model describes the processivity of myosin-V, Biophys. J. 84 (2003) 1642–1650.
[19] P. Xie, S.-X. Dou, P.-Y. Wang, Model for processive movement of myosin V and myosin VI, Chin. Phys. 14 (2005) 744–752.
[20] R. Cooke, Actomyosin interaction in striated muscle, Physiol. Rev. 77 (1997) 671–697.
[21] J.A. Spudich, The myosin swinging cross-bridge model, Nat. Rev. Mol. Cell. 2 (2001) 387–392.
[22] A. Houdusse, H.L. Sweeney, Myosin motors: missing structures and hidden springs, Curr. Opin. Struct. Biol. 11 (2001) 182–194.
[23] S.S. Rosenfeld, J. Xing, L.-Q. Chen, H.L. Sweeney, Myosin IIB is unconventionally conventional, J. Biol. Chem. 278 (2003) 27449–27455.
[24] J.E. Baker, I. Brust-Mascher, S. Ramachandran, L.E.W. LaConte, D.D. Thomas, A large and distinct rotation of the myosin light chain domain occurs upon muscle contraction, Proc. Natl. Acad. Sci. U. S. A. 95 (1998) 2944–2949.
[25] Y.E. Goldman, Wag the tail: structural dynamics of actomyosin, Cell 93 (1998) 1–4.
[26] O. Roopnarine, A.G. Szent-Györgyi, D.D. Thomas, Microsecond rotational dynamics of spin-labeled myosin regulatory light chain induced by relaxation and contraction of scallop muscle, Biochemistry 37 (1998) 14428–14436.
[27] D.M. Warshaw, E. Hayes, D. Gaffney, A.M. Lauzon, J. Wu, G. Kennedy, K. Trybus, S. Lowey, C. Berger, Myosin conformational states determined by single fluorophore polarization, Proc. Natl. Acad. Sci. U. S. A. 95 (1998) 8034–8039.
[28] M. Walker, X.-Z. Zhang, W. Jiang, J. Trinick, H.D. White, Observation of transient disorder during myosin subfragment-1 binding to actin by stopped-flow fluorescence and millisecond time resolution electron cryomicroscopy: evidence that the start of the crossbridge power stroke in muscle has variable geometry, Proc. Natl. Acad. Sci. U. S. A. 96 (1999) 465–470.
[29] N. Volkmann, D. Hanein, Actomyosin: law and order in motility, Curr. Opin. 12 (2000) 26–34.
[30] J. Xu, D.D. Root, Conformational selection during weak binding at the actin and myosin interface, Biophys. J. 79 (2000) 1498–1510.
[31] H.L. Sweeney, A. Houdusse, The motor mechanism of myosin V: insights for muscle contraction, Phil. Trans. R. Soc., B 359 (2004) 1829–1841.
[32] M. Whitaker, E.M. Wilson-Kubalek, J.E. Smith, L. Faust, R.A. Milligan, H.L. Sweeney, 35-Å movement of smooth muscle myosin on ADP release, Nature 378 (1995) 748–751.
[33] J.D. Jontes, E.M. Wilson-Kubalek, R.A. Milligan, A 32 degree tail swing in brush border myosin I on ADP release, Nature 378 (1995) 751–753.

[34] K. Kinosita Jr., M.Y. Ali, K. Adachi, K. Shiroguchi, H. Itoh, How two-foot molecular motors may walk, Adv. Exp. Med. Biol. 565 (2005) 205–219.
[35] F. Kozielski, S. Sack, A. Marx, M. Thormahlen, E. Schonbrunn, V. Biou, A. Thompson, E.-M. Mandelkow, E. Mandelkow, The crystal structure of dimeric kinesin and implications for microtubule-dependent motility, Cell 91 (1997) 985–994.
[36] Y. Li, J.H. Brown, L. Reshetnikova, A. Blazsek, L. Farkas, L. Nyitray, C. Cohen, Visualization of an unstable coiled coil from the scallop myosin rod, Nature 424 (2003) 341–345.
[37] N.B. Becker, S.M. Altmann, T. Scholz, J.K.H. Hörber, E.H.K. Stelzer, A. Rohrbach, Three-dimensional bead position histograms reveal single-molecule nanomechanics, Phys. Rev., E 71 (2005) 021907.
[38] R.A. Mendelson, P.H. Cheung, Intrinsic segmental flexibility of the S-1 moiety of myosin using single-headed myosin, Biochemistry 17 (1978) 2139–2148.
[39] S. Ishiwata, K. Kinosita Jr., H. Yoshimura, A. Ikegami, Rotational motion of myosin heads in myofibril studied by phosphorescence anisotropy decay measurements, J. Biol. Chem. 262 (1987) 8314–8317.
[40] T. Sakamoto, F. Wang, S. Schmitz, Y. Xu, Q. Xu, J.E. Molloy, C. Veigel, J. R. Sellers, Neck length and processivity of myosin V, J. Biol. Chem. 278 (2003) 29201–29207.
[41] F. Wang, L. Chen, O. Arcucci, E.V. Harvey, B. Bowers, Y. Xu, J.A. Hammer III, J.R. Sellers, Effect of ADP and ionic strength on the kinetic and motile properties of recombinant mouse myosin V, J. Biol. Chem. 275 (2000) 4329–4335.
[42] E. Katayama, Quick-freeze deep-etch electron microscopy of the actin-heavy meromyosin complex during the in vitro motility assay, J. Mol. Biol. 278 (1998) 349–367.
[43] P. Xie, S.-X. Dou, P.-Y. Wang, Mechanism for unidirectional movement of kinesin, Chin. Phys. 14 (2005) 734–743.
[44] M. Terrak, G. Rebowski, R.C. Lu, Z. Grabarek, R. Dominguez, Structure of the light chain-binding domain of myosin V, Proc. Natl. Acad. Sci. U. S. A. 102 (2005) 12718–12723.
[45] M.L. Walker, S.A. Burgess, J.R. Sellers, F. Wang, J.A. Hammer, J. Trinick, P.J. Knight, Two-headed binding of a processive myosin to F-actin, Nature 405 (2000) 804–807.
[46] J. Jontes, R.A. Milligan, T.D. Pollard, E.M. Ostap, Biochemical kinetic characterization of brush border myosin I ATPase, Proc. Natl. Acad. Sci. U. S. A. 94 (1997) 14332–14337.
[47] S.S. Rosenfeld, J. Xing, M. Whitaker, H.C. Cheung, F. Brown, A. Wells, R.A. Milligan, H.L. Sweeney, Kinetic and spectroscopic evidence for three actomyosin: ADP states in smooth muscle, J. Biol. Chem. 275 (2000) 25418–25426.
[48] M.D. Wang, M.J. Schnitzer, H. Yin, R. Landick, J. Gelles, S.M. Block, Force and velocity measured for single molecules of RNA polymerase, Science 282 (1998) 902–907.
[49] N.J. Carter, R.A. Cross, Mechanics of the kinesin step, Nature 435 (2005) 308–312.
[50] C.L. Asbury, A.N. Fehr, S.M. Block, Kinesin moves by an asymmetric hand-over-hand mechanism, Science 302 (2003) 2130–2134.
[51] H. Higuchi, C.E. Bronner, H.-W. Park, S.A. Endow, Rapid double 8-nm steps by a kinesin mutant, EMBO J. 23 (2004) 2993–2999.